Label-free microscopy of mitotic chromosomes using the polarization orthogonality breaking technique

Rajesh Desapogu, Gilles Le Marchand, Rebecca Smith, Paulami Ray, Émilie Gillier, Stéphanie Dutertre, Mehdi Alouini, Marc Tramier, Sébastien Huet, Julien Fade

Research Article | Vol. 12, No. 8 / 1 August 2021 / Biomedical Optics Express 5290
Biomedical Optics EXPRESS

Label-free microscopy of mitotic chromosomes using the polarization orthogonality breaking technique

RAJESH DESAPOGU,[1,2,5] GILLES LE MARCHAND,[1,5] REBECCA SMITH,[1] PAULAMI RAY,[2] ÉMILIE GILLIER,[1] STÉPHANIE DUTERTRE,[3] MEHDI ALOUINI,[2] MARC TRAMIER,[1,3] SÉBASTIEN HUET,[1,3,4,6] AND JULIEN FADE[2,7]

[1]*Univ Rennes, CNRS, IGDR, UMR 6290, F-35000 Rennes, France*
[2]*Univ Rennes, CNRS, Institut FOTON–UMR 6082, F-35000 Rennes, France*
[3]*Univ Rennes, BIOSIT, UMS CNRS 3480, US INSERM 018, F-35000 Rennes, France*
[4]*Institut Universitaire de France, France*
[5]*These authors contributed equally to this work*
[6]*sebastien.huet@univ-rennes1.fr*
[7]*julien.fade@univ-rennes1.fr*

Abstract: We report how a recently developed polarization imaging technique, implementing micro-wave photonics and referred to as orthogonality-breaking (OB) imaging, can be adapted on a classical confocal fluorescence microscope, and is able to provide informative polarization images from a single scan of the cell sample. For instance, the comparison of the images of various cell lines at different cell-cycle stages obtained by OB polarization microscopy and fluorescence confocal images shows that an endogenous polarimetric contrast arizes with this instrument on compacted chromosomes during cell division.

1. Introduction

Over the last decades, the relentless development of novel optical imaging techniques addressing specific issues of the biology or biomedical community has given rise to a huge number of unconventional imaging techniques. Several of these were granted with worldwide commercial and scientific success such as Optical Coherence Tomography, advanced confocal fluorescence microscopy, non-linear microscopy, phase microscopy, etc. However, a number of interesting challenges still remain open in this interdisciplinary research field. For some of these challenges, polarimetry can inspire novel solutions to overcome some of the remaining bottlenecks. For instance, the study of cellular biological mechanisms is overwhelmingly performed with confocal laser scanning fluorescence microscopy, which allows the structures of interest to be imaged at high spatio-temporal resolution. Nevertheless, as for any fluorescence-based method, confocal microscopy requires the labeling of the sample using either fluorescent compounds displaying specific localizations whithin the cells, dyes coupled to antibodies or recombinant chimeric constructs composed of a fluorescent protein fused to a protein of interest. Although this labeling step has proven to be usable in multiple contexts, it also suffers some limitations. First, *per se*, it requires an additional, potentially lenghty, step in the sample preparation, thus limiting the throughput of the experiments. Second, due to the crosstalk between the emission spectra of the fluorescent dyes, it is often difficult to image simultaneously more than four different structures within the same sample. Finally, in the context of the observation of living samples, the labeling procedure may induce cytotoxicity and interfere with the tracked biological mechanisms. The development of alternative label-free microscopy methods would alleviate these limitations

#426630 https://doi.org/10.1364/BOE.426630
Journal © 2021 Received 30 Mar 2021; revised 27 May 2021; accepted 29 May 2021; published 28 Jul 2021

Biomedical Optics EXPRESS

and could also provide specific spatial information about the biological samples that would be complementary to those derived from fluorescence imaging.

Among the techniques that are currently investigated (non-linear microscopy, quantitative phase microscopy, diffraction tomography, etc.), polarimetric approaches can provide multidimensional physical information on the samples, which could thus convey also some selectivity in order to identify cell constituents [1–9], investigate the internal organization of biological structures [10–13] or discriminate unhealthy tissues [14–17] without the need for labeling. However, until recently, polarimetric imaging methods pained to widely spread among microscopy systems due to complex calibration and lengthy acquisition procedures of standard polarimetric techniques based on the sequential acquisition of several images [4,10]. Recent progress in polarimetric sensing and imaging enabling fast and sensitive measurements have strongly renewed the interest of the bioimaging community for polarimetric imaging [8,9,18–22].

In this context, another alternative polarimetric imaging modality, referred to as "orthogonality-breaking" (OB) polarimetric sensing has been proposed a few years ago [23–25]. It is based on a microwave photonics approach, and allows different polarimetric properties (birefringence, dichroism, and depolarization) to be identified from a single sample scan using the appropriate detection modality [26]. The first implementations of this original approach on synthetic samples have permitted to confirm its interest, as OB polarimetric sensing offers a mean to access some specific polarization/anisotropy parameters (such as diattenuation coefficient, retardance, anisotropy angle, etc.) and from a single measurement [23–26]. In this paper, we report how such a technique has been implemented on a commercial fluorescence confocal microscope set up in order to provide the instrument with a complementary polarization imaging channel, and how we applied it to cellular imaging. The results presented here demonstrate that this new imaging modality can be used to observe mitotic chromosomes at different stages of the cell division with high contrast and at the spatial resolution allowed by the microscope setup. Being able to monitor such cellular structures can prove useful to quickly identify proliferating cells within a biological sample or to identify cells displaying altered architecture of their genomic material, a feature that is shared by multiple tumor cells [27].

2. Theory

2.1. Principle of orthogonality-breaking polarimetric sensing

OB polarimetric imaging is based on the use of a specific dual-frequency dual-polarization (DFDP) laser illumination to probe the sample. The frequency difference imposed between the two polarization components of equal intensities must lie in the radiofrequency (RF) range, typically 10's to 100's of MHz, in order to match the typical bandwidth of common photodetectors (PD) (photodiodes, avalanche photodiodes (APD), etc.), and avoid chromatic dispersion effects during light propagation in the setup and the sample [23]. It has been shown in earlier theoretical and experimental work on that original technique, that the illumination polarization states should preferably be left/right circular [25] in order to provide the best interpretability of the results. In that case, the fast temporal evolution of the electric field produced corresponds to a linear polarization state rotating at RF frequency. Due to the imposed orthogonality between the two components oscillating at distinct frequencies, the intensity of this DFDP beam has a constant value (DC), even when measured with a fast PD. When such beam propagates through a medium displaying isotropic absorption/scattering properties, the orthogonality between the two polarizations is preserved and therefore, the intensity measured by the PD remains constant. In contrast, interacting with a sample showing some polarization anisotropy will lead to the partial projection of one of the light polarization components onto the other. Due to this orthogonality breaking (OB), the two components of the DFDP beam will interfere and generate an intensity beatnote oscillating at a frequency corresponding to the shift between the two polarizations. This frequency being in the RF range, the beatnote signal (AC) can be detected using fast PDs.

Biomedical Optics EXPRESS

In the OB sensing configuration initally proposed [23], such projection only occurs when light interacts with a dichroic sample (absorption anisotropy) [25,28]. Interestingly, we showed previously that the ratio of the amplitude of the beatnote intensity (I_{AC}) by the average intensity value (I_{DC}), which we shall refer to as orthogonality-breaking contrast (OBC), is a direct measure of the diattenuation rate d of the dichroic sample, since

$$OBC = \frac{|I_{AC}|}{I_{DC}} = d = \frac{T_{max} - T_{min}}{T_{max} + T_{min}}, \tag{1}$$

where the minimum and maximum transmission coefficient of the sample are denoted T_{min} and T_{max} respectively [25,28]. Moreover, the estimated phase of the detected beatnote is directly linked to the direction of the optical anisotropy (here, absorption anisotropy) which is responsible for the OB phenomenon, i.e. $\mathrm{Arg}[I_{AC}] = 2\varphi$, where φ denotes the orientation of the absorption anisotropy [25,28].

The main interest of such OB polarimetric modality is that the polarimetric information is retrieved from a single acquisition (in a pointwise measurement), or a single scan of the image (in an imaging configuration), hence ensuring easy implementation on existing scanning imaging setups such as confocal microscopes. However, the polarimetric information is retrieved from the analysis of a RF-modulated optical signal, which requires fast PDs and dedicated demodulation electronics (lock-in detection or quadrature demodulation board) to measure the in-phase (I_I) and in-quadrature (I_Q) signal components. The OBC and phase informations can be finally retrieved using the following relations:

$$OBC = \frac{\sqrt{I_I^2 + I_Q^2}}{DC}, \qquad \text{and,} \quad \varphi = \frac{1}{2}\mathrm{atan}\frac{I_Q}{I_I}. \tag{2}$$

The requirement of high-speed detection/demodulation hence hinders the use of wide-field cameras, and the technique so far has been implemented in a laser scanning imaging configuration, even for remote measurement applications [29]. For this reason, OB polarimetric sensing is well suited to be implemented on a confocal laser scanning microscope setup, as will be shown in the following.

2.2. Dichroism/birefringence polarimetric imaging with induced-OB modalities

The standard OB imaging modality described above has a strong specificity since OBC contrast can only appear if the sample shows absorption anisotropy (diattenuation). To broaden the scope of application of this unconventional approach, it has recently been shown that it is possible to gain sensitivity on other polarimetric effects, such as pure depolarization and birefringence, by slightly modifying the detection setup [26].

These complementary modalities have been referred to as "induced" OB as the RF beatnote carrying the polarimetric information is generated on an analyzing element placed ahead of the detector, after light has interacted with the sample. Two interesting modalities have been identified. The first one, called linear-induced OB (LI-OB), consists in using a circular left/right DFDP illumination (as described above) and a linear polarizer in front of the detector: this configuration allows depolarization contrasts to be revealed on purely depolarizing samples [26]. The second modality, referred to as circular-induced OB (CI-OB) uses also a circular DFDP illumination, but requires a circular analyzer in front of the detector. This is commonly obtained by combining a quarter-wave-plate (QWP) and a linear polarizer with eigenaxes oriented at 45° from each other. This last modality has the strong potential to reveal interesting OBC contrast, not only on dichroic samples, but also on birefringent samples [26]. More precisely, it was shown that the OBC defined in Eq. (2) provides in that case a direct information about the retardance of

Biomedical Optics EXPRESS

the sample, while the phase of the beatnote still readily indicates the orientation of the anisotropy:

$$OBC = \frac{|I_{AC}|}{I_{DC}} = \sin\delta, \quad \text{and} \quad \text{Arg}[I_{AC}] = 2\varphi, \tag{3}$$

where δ stands for the retardance of the birefringent sample, and φ for the anisotropy orientation.

3. Description of the imaging setup

In this section, we describe how a standard laser scanning microscope (Leica TCS-SP2 inverted microscope setup) has been modified in order to handle OB polarimetric imaging in transmission, while maintaining the ability to perform confocal fluorescence imaging. This constraint was necessary to be able to overlay OB and fluorescence images and thus identify the cellular structures giving rise to the observed polarimetric contrasts. The setup is sketched in Fig. 1(a).

3.1. Dual-frequency dual-polarization illumination

To perform polarimetric cell imaging in the visible range, we use a polarization-sensitive Mach-Zehnder based free-space architecture comprising an acousto-optic shift of 80 MHz in one of the two arms (acousto-optic modulator, MT80-A1-VIS, AA Optoelectronics). This setup is represented on the 3-D sketch of Fig. 1(b) and allows us to obtain a linearly-polarized DFDP beam from a 40 mW commercial blue laser (PC14584, Newport, λ = 488 nm). The DFDP source has previously been extensively described in earlier work [24]. The choice of a frequency-shift in the RF range makes it possible to operate the system with a pixel dwell time compatible with fast image scanning (pixel dwell time of the order of a few microseconds), while ensuring sufficient "averaging" of the RF beatnote that must be precisely quantified to access the polarimeric information. The specific choice of 80 MHz is mainly due to the commercial availability of acousto-optic frequency shifters at such frequency which fullfills the above condition.

In order to control the optical power deposited on the sample, a mechanically controlled optical valve has been designed using the association of a half-wave plate (HWP) (WPHSM05-488, Thorlabs) and a Glan polarizer inserted between the laser output and the Mach-Zehnder-like setup. The orientation of the Glan polarizer is adjusted to ensure that the intensity of the two components of the DFDP beam share equal intensities. The direction of the HWP is controlled by a rotating mount (URS50 + SMC100 controller, Newport), allowing remote tuning of the optical power from the LabVIEW (National Instruments) program used to control the whole setup.

In order to convey the DFDP beam into the microscope scanning head, we use a single mode polarization-maintaining optical fiber (P3-488PM-FC-2, Thorlabs) whose eigenaxes have been aligned with the polarization directions of the DFDP beam. A mechanical shutter controlled by the LabVIEW software is placed ahead of the fiber injection and avoids illumination of the sample before an acquisition is launched, so as to reduce fluorescence bleaching.

3.2. Microscope setup

The DFDP beam conveyed by the fiber is coupled into the confocal microscope (TCS-SP2, Leica) through the original infrared port using a dichroic mirror (ZT488rdc, Chroma, cut-off wavelength 498 nm), as sketched in Fig. 1(a). This makes it possible to perform fluorescence and polarimetric imaging simultaneously, as the excitation laser lines available in the confocal head (514 nm and 633 nm) can be used to illuminate the sample and the fluorescence emitted in the backward direction can be detected through the confocal pinhole. The filter wheel of the inverted microscope stand has been equipped with a removable QWP at 488 nm (WPQSM05-488, Thorlabs), allowing the linear DFDP beam to be converted into a circular left/right DFDP illumination at the sample plane. Finally, the light is focused onto the sample by the microscope objective, with a typical optical power of the DFDP beam of 4 mW to produce the images. To

Biomedical Optics EXPRESS

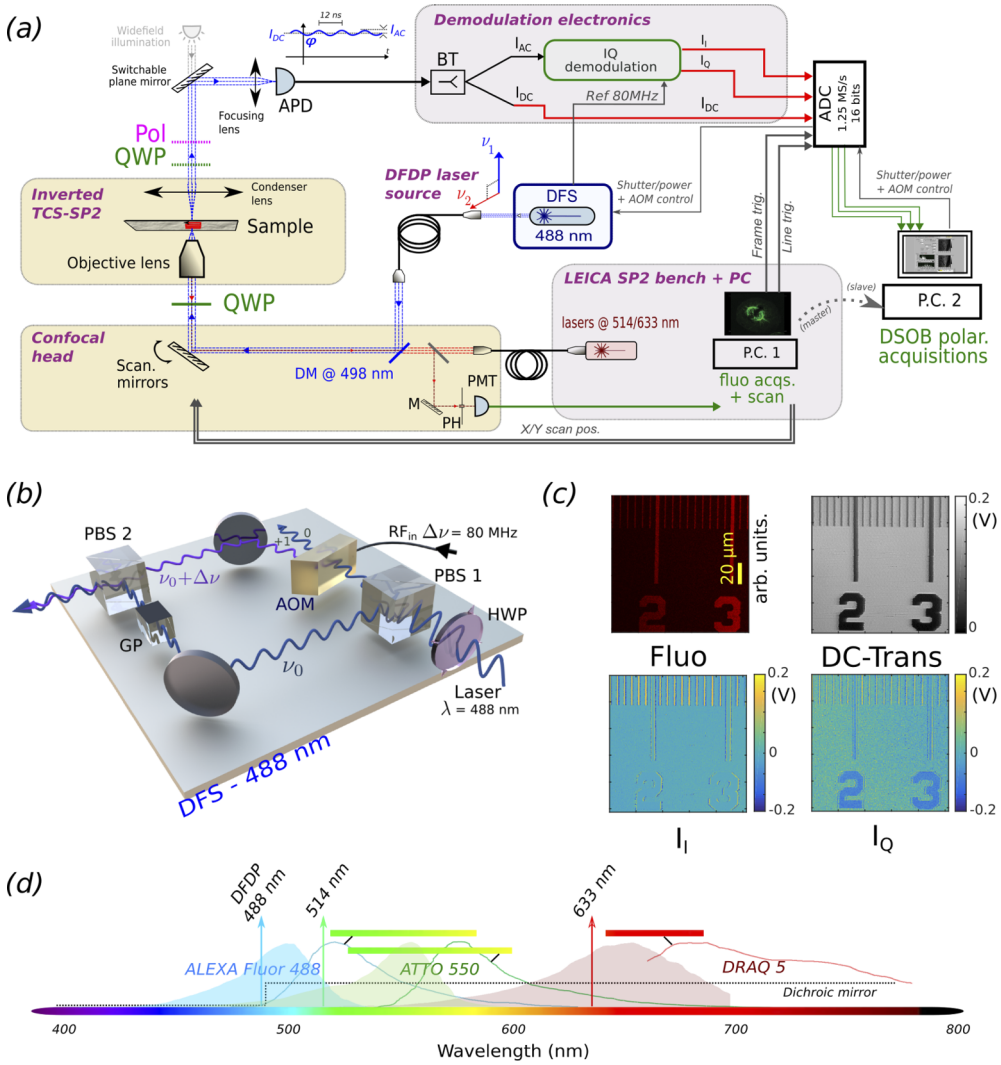

Fig. 1. (a) Sketch of the OB polarimetric microscope setup implemented on a standard fluorescence scanning microscope (Pol: polarizer, QWP: quarter-wave plate at 488 nm, APD: avalanche photodiode, BT: bias-tee, DFS: dual-frequency source, DM: dichroic mirror, PH: pinhole, PM: photomultiplier). (b) 3D-sketch of the dual-frequency dual-polarization laser source at λ=488 nm designed for the experiment (HWP: half-wave plate, PBS: polarization beam splitter, AOM: acousto-optic modulator, GP: Glan polarizer). (c) Example of test images recorded from the fluorescence confocal microsope (Fluo), and from the polarimetric acquisition setup: the DC image provides the transillumination image, the I and Q channels are further processed to build the OBC and phase images displayed in next figures. (d) Alexa Fluor 488, ATTO 550 and DRAQ5 absorption/emission spectra and fluorescence detection spectral windows are represented as a function of wavelength along with used laser lines and dichroic mirror spectrum.

Biomedical Optics EXPRESS

minimize the effect of spurious polarimetric effects due to the used optics (mirrors, multiple lens set in the objective lens), a half-wave plate at 488 nm was used (WPH10M-488, Thorlabs) to ensure exact alignment of the linear polarization directions of the input beam conveyed by the optical fiber with the incidence plane on the mirrors (including scanning mirrors). With such caution, the extinction ratio of the two linear polarizations reached ~ 500 : 1 at the focal plane, and upon propagation through the QWP, the measured ellipticity of the circular polarization was 43° ± 1°. All the images shown below have been recorded with one of the two following objectives: a 10× objective (Leica HCXPL APO 10×/0.40 CS, NA=0.4) for test images and polarimetric measurements on synthetic samples (Fig. 2), whereas the images of cells have been obtained with an oil-immersion 63× objective (Leica HCXPL APO 63×/1.40-0.60 OIL CS, NA=1.4). It must be noted here that no undesirable contribution or artifact was observed on the OB polarimetric signatures, even though a high NA objective − known to potentially affect the light polarization − was used: indeed, even without any sample at the focalization plane, no further increase of the OB ground level was observed on the edges of the acquired images, that could have indicated such polarimetric artifact due to high focalization.

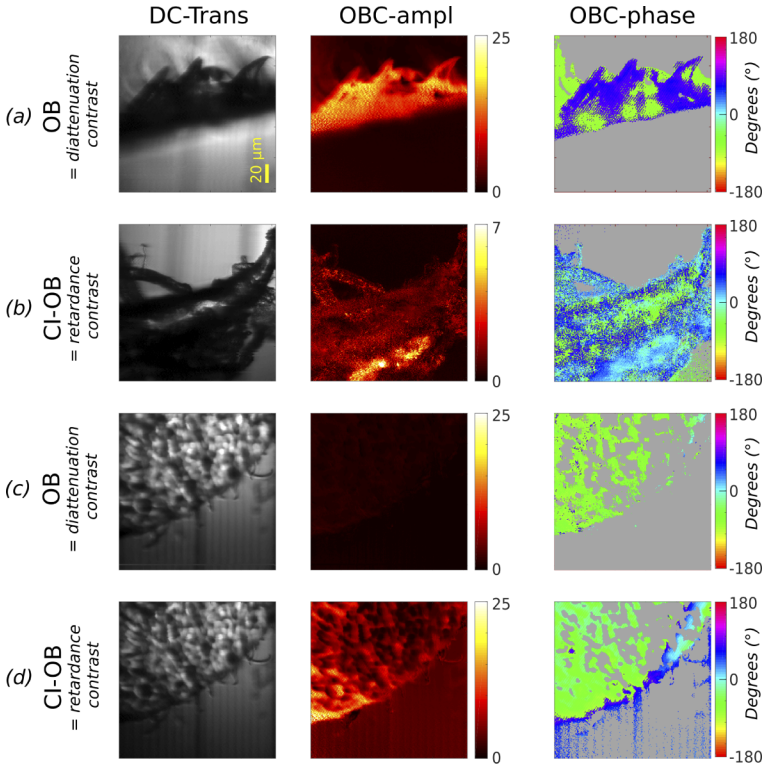

Fig. 2. Examples of OB polarimetric images recorded with a 10× objective on synthethic samples. Left column: DC-transillumination image; Center: OBC amplitude map; Right: OBC phase map. (a): diattenuation contrast (OB-modality) on the edge of a dichroic sample (tears of polaroid sheets); (b): retardance contrast (CI-OB modality) on a similar sample to (a); (c): diattenuation contrast (OB-modality) on cuts of a birefringent sample (plastic tape); (d): retardance contrast (CI-OB modality) on the same sample as in (c).

Upon interaction with the sample, light is detected on the one hand in the classical confocal backscattering mode for the fluorescence emission, and the image reconstruction is handled by the TCS-SP2 system. On the other hand, the polarization information is measured in transmission by detecting the OB beatnote at 80 MHz on an avalanche photodiode (APD) (Silicium, 400 MHz

Biomedical Optics EXPRESS

bandwidth, APD430A, Thorlabs), through a custom optical arrangement comprising the original microscope condenser lens (f'=28 mm), a switchable plane mirror, and an additional focusing lens (f'=17 mm) (See Fig. 1(a)). Despite the fact that transmitted beam is not de-scanned before detection on the APD, the diameter of the latter combined to a slight defocus of the condenser is sufficient to ensure the detection of a uniform field up to $\sim 100 \times 100\ \mu m^2$. This configuration enables full operation of the Leica microscope in its original mode (including widefield top illumination), but hinders the ability of true simultaneous imaging since a slight tuning of the microscope focus must be ensured when switching between confocal fluorescence imaging and polarimetric OB imaging. Moreover, although the polarimetric channel does not benefit from the optical sectioning offered by the confocal detection, the lateral resolution of the images was observed to be comparable with both modalities, i.e., of the order of $\simeq 100 - 200$ nm within the focal plane with the 63× oil-immersion objective.

Finally, in order to implement the three OB modalities described above, removable polarization analysis elements have been inserted after the sample, between the condenser lens and the last focusing lens. A linear polarizer allows LI-OB to be performed, while CI-OB requires an additional QWP to be inserted before the polarizer, with eigenaxes oriented at 45° from the polarizer direction.

3.3. Polarimetric data acquisition and image reconstruction

As described in the theoretical section, OB polarimetric imaging requires a specific detection and demodulation chain to recover the polarimetric information from the estimated amplitude and phase of a RF beatnote, at 80 MHz in the present case. For that purpose, a first homemade "bias-tee" electronic circuit separates the 80 MHz AC component of the detected photocurrent from its continuous-wave DC component. As sketched in Fig. 1(a), the latter is directly sampled and digitized on the analog-to-digital conversion (ADC) module of an input/output board (NI-USB 6356, National Instruments, 16 bits, 1.25 MS/s per channel).

As for the AC component, it can be demodulated either with a lock-in amplifier [24], or using a custom-made I/Q demodulation circuit at the dedicated 80 MHz frequency. Here, we use the I/Q demodulation approach which has been extensively described in previous work [29]. On our microscope setup, the RF reference (local oscillator) used to demodulated the AC photocurrent is given by the 80 MHz RF signal that drives the acousto-optic modulator, with appropriate amplification to match the nominal operating point of the RF mixers (+7 dBm) involved in the demodulation circuit. At the output of the I/Q demodulation circuit, the two quadratures (I and Q) are low-pass filtered (1 MHz cutoff frequency) and further amplified using two identical switchable gain voltage amplifiers (from ×3 to ×34) so as to optimally match the input range of the ADC board which eventually samples and digitizes the I and Q signals along with the DC component.

The three digitized signals are then processed with a LabVIEW program on a computer to build the three raw polarimetric images (DC, I, Q), from which the OBC amplitude and phase maps are computed using the relations of Eq. (2), taking into account the relative gain factors and input ranges of the three channels. Data acquisition and reconstruction of the images are triggered by the "frame" and "line" trigger signals from the Leica bench which are also digitized on the ADC board. In addition, to avoid photodamage or bleaching of the sample and to minimize aging of the AOM, a +5V signal is output from the I/O board only when the acquisition is started, in order to open the mechanical shutter of the DFDP source and to enable the RF high-voltage supply of the AOM.

Using a 200 Hz scanning speed on the Leica system allows polarimetric images of 256×256 pixels to be recorded within 1.5 s. In order to cope with the acceleration/deceleration phases of the galvanometric mirrors and avoid spatial distortion in the obtained images, the simplest way consists in acquiring an image format of 512×256 pixels and remove by software the 128

Biomedical Optics EXPRESS

first and last pixels from each line, ending up with distorsion-free 256 × 256 pixel images. An example of raw DC, I and Q images recorded with a ×10 objective on a stage micrometer is displayed in Fig. 1(c), along with the corresponding fluorescence image.

For the sake of accuracy of the estimated OBC amplitude and phase maps, the I and Q images displayed in the following figures and used to compute the OBC amplitude and phase values have been corrected by software from slow phase drifts due to unwanted optical path changes in the DFDP source. For that purpose, we estimate the slow drift on the quadrature images by evaluating the local average values of the I and Q signals at four locations around the cell (typically, the four image corners), and by using a linear regression to calculate the slow linear trend of the I/Q signals across the image. This slow trend is finally removed to provide the I and Q images as those displayed in Fig. 3(c). Such post-processing steps could be avoided in future implementation of the system by removing the unwanted optical phase drifts in the system.

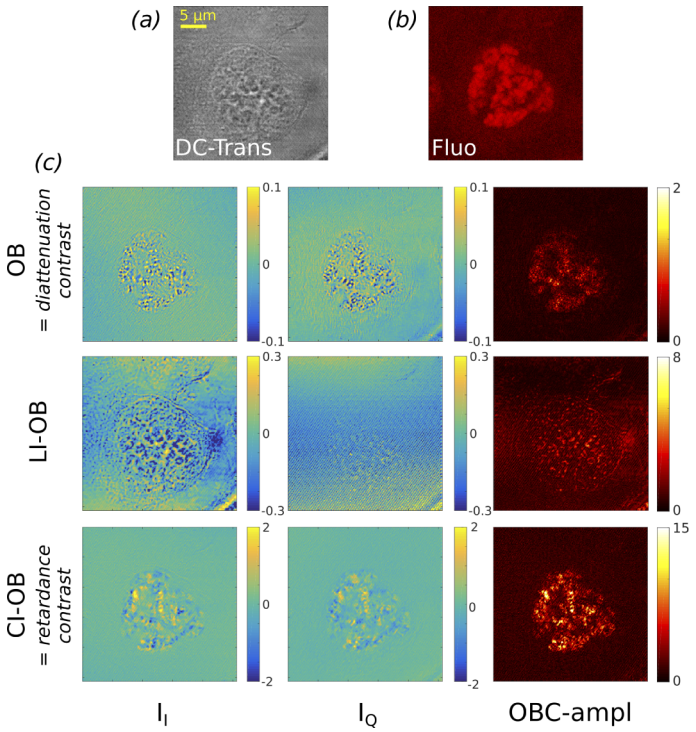

Fig. 3. Fluorescence and OB polarimetric images of a U2OS cell whose DNA has been labeled with DRAQ5. Images were obtained with a 63× oil-immersion objective. (a) Transillumination image; (b) Fluorescence image; (c) OB polarimetric images with I/Q channels and OBC amplitude maps for standard OB modality (diattenuation contrast, upper row); linear-induced OB (middle row) and circular-induced OB (retardance contrast, lower row).

3.4. Sample cells preparation and fluorescence imaging

HeLa and U2OS cells were cultured in Dulbecco's Modified Eagle's Medium (DMEM) supplemented with 10% fetal bovine serum (FBS), 100 μg/mL penicillin and 100 U/mL streptomycin and maintainted at 37°C in a 5% CO_2 incubator. Cells were seeded on coverslips 24 h prior to fixation. For DRAQ5 staining (U2OS cells), media was removed and cells were washed once with phosphate buffered saline (PBS) for 3 min at room temperature. Cells were fixed in 4%

Biomedical Optics EXPRESS

paraformaldehyde (PFA) for 15 min at room temperature and washed twice with PBS. Cells were stained with DRAQ5 (0.5 mM in PBS) for 15 minutes and washed three times with PBS before coverslips were mounted on slides using ProLong Gold (Thermo Fisher Scientific). The U2OS cells displayed in the lower row of Fig. 4 were stained with Phalloidin-ATTO 550 (Sigma Aldrich) used at 0.1 nmol/mL to highlight the actin cytoskeleton.

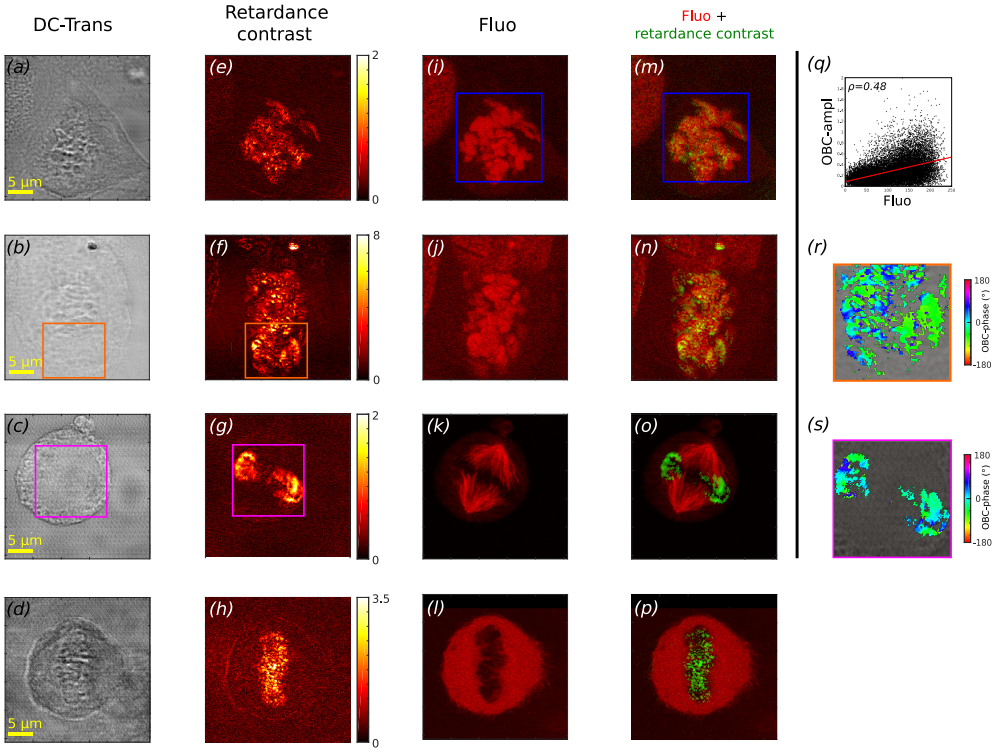

Fig. 4. Comparison of transillumination (a-d), retardance-OBC (e-h) and fluorescence (i-l) images acquired on U2OS cells labeled with DRAQ5 to highlight the DNA in fluorescence (upper and second row), on HeLa cells whose microtubules were labeled by immunofluorescence and DNA was stained with Hoechst (third row, Hoechst staining not shown), and on U2OS cells whose actin cytoskeleton was labeled by fluorescent phalloidin but whose DNA was left unstained (lower row). In each case, the superimposition of the fluorescence and retardance-OBC images displayed in (m-p) shows clear colocalization between the OBC contrast and the compacted chromatin in mitotic cells. The colocalization in the blue ROI in the first row is confirmed by the cytofluorogram displayed in (q), where ρ stands for the correlation coefficient between OBC amplitude values and fluorescence signal levels. The two thumbnails (r) and (s) show two examples of phase maps extracted from the retardance-OB images revealing additional morphological contrasts on the compacted chromatin.

For microtubule staining (HeLa cells), media was removed and cells were washed once with PBS for 3 min, fixed with 4% PFA for 15 min and washed twice with PBS, all performed at room temperature. Cells were permeabilized with 0.2% Triton X-100 in PBS for 5 min, washed twice with PBS and placed in blocking buffer (5% BSA, 0.05% Tween-20 in PBS) for 60 min at room temperature. Cells were then incubated with anti-tubulin antibody (0.2 μg/mL, sc #62204, Invitrogen) in blocking buffer overnight at 4°C. Cells were washed three times with 0.1% Triton X-100 in PBS before incubation with Alexa Fluor 488 anti-mouse IgG (2 μg/mL, A11001, Invitrogen) diluted in blocking buffer at room temperature for 1 h in the dark. Cells

Biomedical Optics EXPRESS

were washed twice with 0.1% Triton X-100 in PBS and counterstained with Hoechst (1 μg/mL in PBS) for 10 minutes. Cells were washed three times with PBS before coverslips were mounted on slides using ProLong Gold.

Alexa Fluor 488 and ATTO 550 were excited using the 514 nm laser line, whereas the 633 nm line was used for DRAQ5. For fluorescence detection, we used bandpass filters adapted to the fluorophore emission spectra (respectively [520 – 580] nm for Alexa Fluor 488, [520 – 600] nm for ATTO 550, and [640 – 680] nm for DRAQ5). The absorption/emission spectra of Alexa Fluor 488, ATTO 550 and DRAQ5 are represented in Fig. 1(d), along with the excitation laser lines and the fluorescence detection spectral windows used.

4. Results and discussion

4.1. Validation on synthetic samples

Before applying the OB polarimetric imaging to cell samples, we validated the method and the setup on synthetic test samples. These samples were selected for their known anisotropic optical behaviour, such as dichroism and birefringence, and the obtained images displayed in Fig. 2 are in good agreement with the theory presented above and in earlier Ref. [26]. In this figure, the left column shows the transillumination image obtained with a $\times$10 objective from the measured DC signal of the APD, while the center and right column respectively display the OBC amplitude and phase maps obtained from Eq. (2). The phase value being irrelevant when the AC amplitude is very low (i.e., low OBC), the phase map has been thresholded and the irrelevant phase values have been represented in gray color. Some striation of the images can be oberved in the polarimetric channels (see Fig. 2(d) for instance, and subsequent figures), which is due to low-frequency (1 – 10 kHz range) parasitic noise detected by the APD and electronic demodulation board. Improved RF shielding of these components would prevent this spurious striation effect on the images. Moreover, it must be noted that so far the amplitude values of the OBC maps are not quantitatively calibrated in terms of absolute diattenuation/retardance units. This does not prevent however comparative evaluation of the imaging data gathered on biological samples, as presented below. Perfect quantitative calibration and linearization of the OBC signal in diattenuation/retardance would require added complexity to the system, and involves complex and tedious calibration procedure and data post-processing [26,30], which is outside the scope of the present paper.

The images in the first two rows have been obtained on a dichroic sample, namely, the cut edges of a polaroid sheet deposited on the stage micrometer surface, and exhibiting a rather shredded structure. The diattenuation contrast measured by standard OB imaging modality is shown in Fig. 2(a), whereas images of Fig. 2(b) display retardance contrast obtained with the circular-induced modality. As expected, the in-focus parts of the dichroic sample show strong OBC with the two OB modalities. Theoretically, the estimated phase provides an indication about the relative orientation of the absorption anisotropies in the observed sample. The phase maps obtained here showing different values on the polarizer shreds are in fair agreement with the expected behaviour.

The second synthetic sample tested corresponds to a piece of plastic tape sticked on the stage micrometer. The piece of tape is clearly visible in the upper-left corner of the transillumination image of Figs. 2(c) and 2(d). It has been imaged here with the standard OB (Fig. 2(c)) and the CI-OB modalities (Fig. 2(d)). Again, as expected based on the theory, such a birefringent sample does not break the polarimetric orthogonality, hence resulting in a very low OBC amplitude in standard OB. However, the birefringent nature of the sample clearly appears through the significant OBC amplitude obtained on the birefringent sample with the CI-OB modality. As for the phase maps, the constant value of the phase estimated on the piece of tape is in good agreement with the expected uniform orientation of the phase anisotropy of such sample. These first imaging results on test synthetic samples confirm the expected specificity of the OB sensing

Biomedical Optics EXPRESS

modalities to different polarimetric effects. The results of Fig. 2 also validate the correct operation of the polarimetric OB microscope.

4.2. OB polarimetric observations in cells

We imaged human osteosarcoma U2OS cells using the confocal fluorescence modality of the TCS-SP2 Leica system, and compared the fluorescence images with the transillumination (DC) and polarimetric images (OBC amplitude and phase maps) acquired using the method and system described above. An interesting outcome of these experiments is the observation of an intrinsic polarimetric OBC in mitotic cells. An example of such acquisition is displayed in Fig. 3, where a U2OS cell, stained with DRAQ5 for DNA fluorescence labeling, has been imaged with the confocal fluorescence microscope (Fig. 3(b)), and with the three OB modalities (Fig. 3(c)). The spatial distribution of the chromosomes within this cell as seen on the fluorescence image suggests that it is at an early mitotic stage, most probably prometaphase. The analysis of the raw polarimetric images (I and Q) shows that a diattenuation contrast can be observed in standard OB imaging modality (first raw of Fig. 3(c)). Such contrast seems to arise at compacted chromatin, as shown by the fact that the spatial distribution of the OBC signal (right column in Fig. 3(c)) resembles the fluorescence image. The linear-induced OB modality (LI-OB) does not reveal significant depolarization contrast (middle row), as could be expected from such a thin and transparent sample for which light depolarization induced by multiple scattering events during light propagation is unlikely. In contrast, the circular-induced modality (CI-OB), which was previously shown to be also sensitive to retardance constrast [26], gives rise to the strongest I and Q quadrature signal contributions, and makes it possible to retrieve a clear OBC amplitude map (lower row, right) with high signal-to-noise ratio. For this reason, we shall restrict ourselves in the following to this CI-OB modality, which seems best adapted to the imaging of compacted chromatin in mitotic cells. However, the fact that an OBC can be simultaneously observed in the standard OB modality and in the CI-OB modality, with stronger magnitude in the latter, seems to indicate that the observed contrast is apparently due to a complex mixture or interplay of both diattenuation and retardance effects in the imaged structure. For the sake of clarity however, this CI-OB contrast will be referred to as "retardance"-OBC in the following figures and in the remainder of the article.

4.3. Label-free polarimetric contrast of mitotic chromosomes

The clear contrast obtained in a dividing U2OS cell such as presented in Fig. 3(c) (third row) is very encouraging towards the possibility to identify mitotic chromosomes from an endogenous polarimetric contrast, without the need for fluorescence labeling. It was however important to verify that such contrast was not specific to this cell line and not due to the DRAQ5 labeling of the DNA. Moreover, a more thorough analysis was required to confirm that the polarimetric contrast colocalizes with the mitotic chromosomes.

For this purpose, we performed some additional acquisitions in two types of cells: U2OS cells, described in the previous section, and HeLa cells, a widely used human cancer cell line derived from cervix. These cells were labeled either with DRAQ5, to highlight the DNA (U2OS cells), or with an anti-tubulin antibody, to display the microtubule network (HeLa cells). We imaged cells undergoing mitosis in both OB retardance contrast and fluorescence modalities and the two images were overlapped to be able to assess the colocalization between the two signals. The results are displayed in Fig. 4. It can be readily observed in Fig. 4(m) and 4(n) that the retardance-OBC map overlaps very well with the strong fluorescence signal emitted by the DRAQ5 dye labeling the chromatin. This is confirmed by the cytofluorogram displayed in Fig. 4(q), which is obtained from the blue ROI of the first U2OS cell (upper row). When imaging a dividing HeLa cell which microtubules were tagged by immunofluorescence, we observed in Fig. 4(d) the overlay between the retardance-OBC (in green) and the fluorescence (in red) signals,

Biomedical Optics EXPRESS

a characteristic metaphase spindle composed of microtubules (seen in fluorescence) handling mitotics chromomes (seen in the polarimetric channel, as was the case with the previously presented U2OS cells). This last result demonstrates that the polarimetric contrast observed for the mitotic chromosomes is not specific to a single cell type and is not due to DNA labeling by DRAQ5, hence paving the way to label-free imaging of mitotic chromosomes in dividing cells. To further confirm this result, we also performed OB imaging on U2OS cells with unstained DNA: the transillumination image and OBC map respectively displayed in Fig. 4(d) and Fig. 4(h) clearly confirm that the observed contrast is not due to fluorescence labelling of DNA.

The results of Fig. 4 deserve discussion, as they seem to contradict anterior studies in polarized cell microscopy that demonstrated the strong birefringent properties of the microtubule network [1–5]. In our experiments, such structures where never observed in none of the three OB modalities described above. This can be due to a lack of sensitivity of our instrument, but most probably due to the imaging conditions (laser scanning imaging in transmission, choice of the mounting medium, etc.) that strongly differ from those involved in these references. On the other hand, our observations are in agreement with recent works [8,9] that reported the observation of a polarimetric signature in DNA/chromatin using a differential circular polarization microscopy technique. Once again, we do not claim at this stage that the contrast observed in the so-called retardance-OBC maps is a clear manifestation of linear birefringence, especially in the compacted chromatin, since it also (more slightly) shows up in the diattenuation-OBC map (see Fig. 3(c) (upper row)). The origin of this polarimetric signature in chromatin will be rigorously investigated in future work, where the specificity of the chromatin response in the CI-OB modality should be questioned, as well as the highlighting of other cell structures with OB imaging in general.

In addition to the retardance-OBC maps whose amplitude seems to be related to chromatin compaction, the OB polarimetric techniques provide additional information by analyzing the estimated phase of the OB signal at each pixel of the image [26]. Two examples of phase maps (estimated only on pixels showing significant OBC amplitude) are displayed for a U2OS cell (Fig. 4(r)) and a HeLa cell (Fig. 4(s)). Interestingly, these two phase images reveal additional morphological information in the compacted chromatin that can be observed neither in the retardance-OBC maps nor in the fluorescence images. Further investigation is required to possibly relate such observations with morphological/organizational structures in compacted chromosomes [31].

As a last experiment to confirm the interest of such endogenous polarimetric contrast in condensed chromatin, we provide in Fig. 5 a comparison of the transillumination (upper row), OBC amplitude (retardance contrast, middle row) and fluorescence (lower row) images of U2OS cells at different cell stages. From left to right, the analysis of fluorescence images allows us to identify cells in interphase (a), late prophase (b), prometaphase (c), late prometaphase (d), metaphase (e), and finally late telophase (f). This figure shows that the polarimetric contrast seems to only arize at compacted chromatin in cells undergoing mitosis, while no clear OBC could be observed in interphase cells (Fig. 5(a)). On a more quantitative basis, the magnitude of the OB polarimetric contrast seems to follow the chromatin compaction during the mitotic process, suggesting that OB imaging could be used to monitor the chromatin compaction state. This is confirmed by the graph displayed at the bottom of Fig. 5, which shows the ratio between the OBC amplitude averaged over the regions of interest (ROIs) highlighted in blue, and its mean value in the surrounding background. The selected ROIs correspond to the regions where labeled DNA can be identified in the fluorescence images.

Lastly, we emphasize that such results were consistent over many cells observed in the samples: similar chromatin compaction was observed in all the dividing cells (that were identified from the fluorescence labelled image), and with varying spatial orientation of the mitotic stage. However, for the sake of conciseness, all the imaging results could not be reported here, and a statistical study over a wide population of cells is outside the scope of this paper.

Biomedical Optics EXPRESS

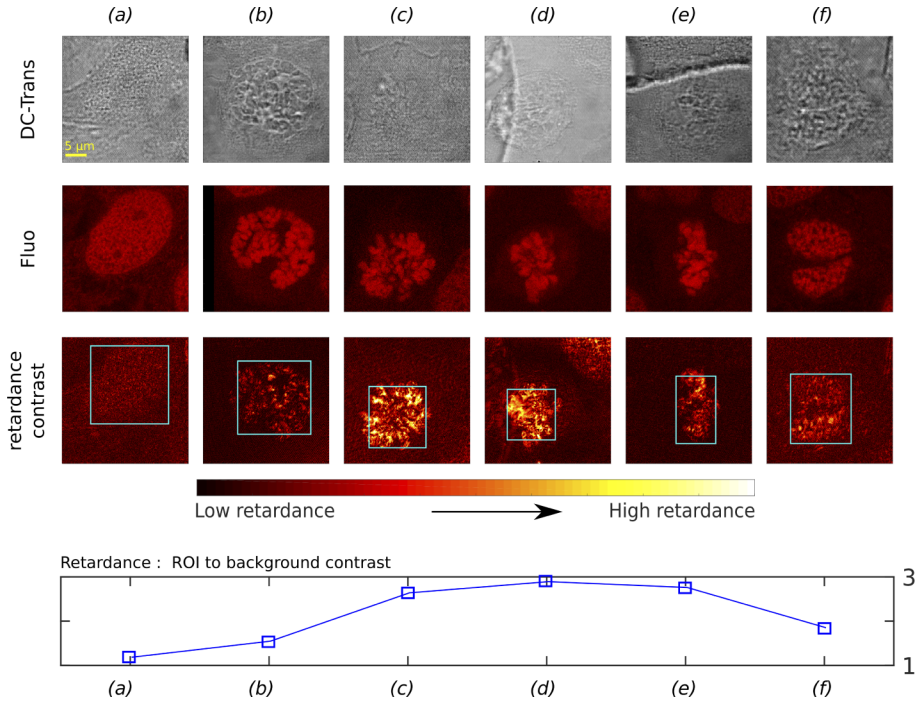

Fig. 5. Transillumination, fluorescence and OBC amplitude (circular-induced OB) images of DRAQ5 labeled U2OS cells at different cell stages: (a) interphase; (b) late prophase; (c) prometaphase; (d) late prometaphase; (e) metaphase and (f) late telophase. Bottom plot: evaluation of the ROI-to-background contrast of the averaged OBC amplitude on the regions displaying DNA in the fluorescence images (blue ROIs).

5. Conclusion

In this article, we have shown that polarized microscopy using "orthogonality breaking" approaches could provide valuable label-free information in biological samples. More specifically, it has been shown that an endogenous polarimetric "circular-induced" OB contrast revealing birefringence properties (retardance) of the sample could be obtained at mitotic chromosomes during cell division, which has been confirmed by colocalization with fluorescence images recorded on the same samples. As the polarimetric modality used in this study only requires a single scan of the sample, this technique has the potential to allow live cell imaging to monitor chromosome dynamics during mitosis. In this context, modifying the microscope setup to enable imaging in a reflection configuration would ensure strict simultaneous fluorescence and polarization live-cell imaging.

Applying this label-free technique to study the chromatin compaction state could open promising perspective for histology studies, such as the identification of abnormal chromatin compaction arising in some cancers cells [32,33]. Further investigation is being conducted to assess the interest of this approach for imaging other cellular structures, or other kinds of cell samples such as embryos [34,35], or biological tissues. This next experimental work will also address the thorough and rigorous calibration of the setup in order to provide more reliable quantitative assessments of the estimated diattenuation/retardance magnitude and orientation maps, which can be of great interest to investigate the interesting morphological structures revealed by these complementary contrasts.

Biomedical Optics EXPRESS

Funding. Agence Nationale de la Recherche (ANR-10-INSB-04); Campus France (PRESTIGE PRESTIGE-2017-2-0042).

Acknowledgments. The authors would like to acknowledge N. Ortega-Quijano, F. Parnet for their early contribution in OB imaging, and to thank L. Frein, S. Bouhier, C. Hamel, and A. Carré for their technical help with the electronical and mechanical design of the experiments. The authors thank C. Chapuis for her technical assistance in sample preparation and X. Pinson for his technical help with the confocal microscope setup. The authors thank the MRic facility from the BIOSIT joint unit of services, the University of Rennes 1 and the CNRS *"Mission pour les Initiatives Transverses et Interdisciplinaires"* (MITI) for funding this project. R.D. was supported by the Université Bretagne Loire, the Région Bretagne and the Institut Universitaire de France. R.S. was supported by the PRESTIGE program coordinated by Campus France [PRESTIGE-2017-2-0042], the Université Bretagne Loire and the Fondation ARC pour la recherche sur le cancer [PDF20181208405]. We thank the GDR Imabio for funding P.R.'s and E.G.'s internships. The MRic facility is member of the national infrastructure France-BioImaging supported by the French National Research Agency (ANR-10-INSB-04).

Disclosures. The authors declare no conflicts of interests.

Data availability. Data underlying the results presented in this paper are not publicly available at this time but may be obtained from the authors upon reasonable request.

References

1. R. Oldenbourg, "A new view on polarization microscopy," Nature **381**(6585), 811–812 (1996).
2. R. Oldenbourg, "Polarized light microscopy of spindles," Methods Cell Biol. **61**, 175–208 (1998).
3. S. Inoué and R. Oldenbourg, "Microtubule dynamics in mitotic spindle displayed by polarized light microscopy," Mol. Biol. Cell **9**(7), 1603–1607 (1998).
4. J. R. Kuhn, Z. Wu, and M. Poenie, "Modulated polarization microscopy: a promising new approach to visualizing cytoskeletal dynamics in living cells," Biophys. J. **80**(2), 972–985 (2001).
5. S. Inoué, "Microtubule dynamics in cell division: exploring living cells with polarized light microscopy," Annu. Rev. Cell Dev. Biol. **24**(1), 1–28 (2008).
6. A. Morimoto, S. Matsunaga, D. Kurihara, and K. Fukui, "Visualization of mitotic hela cells by advanced polarized light microscopy," Micron **39**(5), 635–638 (2008).
7. C. Zheng, G. Zhao, W. Liu, Y. Chen, Z. Zhang, L. Jin, Y. Xu, C. Kuang, and X. Liu, "Three-dimensional super-resolved live cell imaging through polarized multi-angle tirf," Opt. Lett. **43**(7), 1423–1426 (2018).
8. A. L. Gratiet, L. Pesce, M. Oneto, R. Marongiu, G. Zanini, P. Bianchini, and A. Diaspro, "Circular intensity differential scattering (cids) scanning microscopy to image chromatin-dna nuclear organization," OSA Continuum **1**(3), 1068–1078 (2018).
9. R. Marongiu, A. L. Gratiet, L. Pesce, P. Bianchini, and A. Diaspro, "Excids: a combined approach coupling expansion microscopy (exm) and circular intensity differential scattering (cids) for chromatin-dna imaging," OSA Continuum **3**(7), 1770–1780 (2020).
10. N. Ghosh and A. I. Vitkin, "Tissue polarimetry: concepts, challenges, applications, and outlook," J. Biomed. Opt. **16**(11), 110801 (2011).
11. S. Brasselet, "Polarization-resolved nonlinear microscopy: application to structural molecular and biological imaging," Adv. Opt. Photonics **3**(3), 205 (2011).
12. P. G. Ellingsen, L. M. S. Aas, V. S. Hagen, R. Kumar, M. B. Lilledahl, and M. Kildemo, "Mueller matrix three-dimensional directional imaging of collagen fibers," J. Biomed. Opt. **19**(2), 026002 (2014).
13. S. Alali and A. Vitkin, "Polarized light imaging in biomedicine: emerging Mueller matrix methodologies for bulk tissue assessment," J. Biomed. Opt. **20**(6), 061104 (2015).
14. J. Chung, W. Jung, M. J. Hammer-Wilson, P. Wilder-Smith, and Z. Chen, "Use of polar decomposition for the diagnosis of oral precancer," Appl. Opt. **46**(15), 3038–3045 (2007).
15. E. Salomatina-Motts, V. Neel, and A. Yaroslavskaya, "Multimodal polarization system for imaging skin cancer," Opt. Spectrosc. **107**(6), 884–890 (2009).
16. A. Pierangelo, A. Benali, M.-R. Antonelli, T. Novikova, P. Validire, B. Gayet, and A. De Martino, "Ex-vivo characterization of human colon cancer by Mueller polarimetric imaging," Opt. Express **19**(2), 1582–1593 (2011).
17. A. Pierangelo, S. Manhas, A. Benali, C. Fallet, J.-L. Totobenazara, M. R. Antonelli, T. Novikova, B. Gayet, A. De Martino, and P. Validire, "Multispectral Mueller polarimetric imaging detecting residual cancer and cancer regression after neoadjuvant treatment for colorectal carcinomas," J. Biomed. Opt. **18**(4), 046014 (2013).
18. J. Qi and D. S. Elson, "Mueller polarimetric imaging for surgical and diagnostic applications: a review," J. Biophotonics **10**(8), 950–982 (2017).
19. M. W. Kudenov, M. J. Escuti, N. Hagen, E. L. Dereniak, and K. Oka, "Snapshot imaging Mueller matrix polarimeter using polarization gratings," Opt. Lett. **37**(8), 1367–1369 (2012).
20. A. L. Gratiet, M. Dubreuil, S. Rivet, and Y. L. Grand, "Scanning Mueller polarimetric microscopy," Opt. Lett. **41**(18), 4336–4339 (2016).
21. B. Bai, H. Wang, T. Liu, Y. Rivenson, J. FitzGerald, and A. Ozcan, "Pathological crystal imaging with single-shot computational polarized light microscopy," J. Biophotonics **13**(1), e201960036 (2020).
22. A. Le Gratiet, A. Mohebi, F. Callegari, P. Bianchini, and A. Diaspro, "Review on complete Mueller matrix optical scanning microscopy imaging," Appl. Sci. **11**(4), 1632 (2021).

Biomedical Optics EXPRESS

23. J. Fade and M. Alouini, "Depolarization remote sensing by orthogonality breaking," Phys. Rev. Lett. **109**(4), 043901 (2012).
24. E. Schaub, J. Fade, N. Ortega-Quijano, C. Hamel, and M. Alouini, "Polarimetric contrast microscopy by orthogonality breaking," J. Opt. **16**(12), 122001 (2014).
25. N. Ortega-Quijano, J. Fade, E. Schaub, F. Parnet, and M. Alouini, "Full characterization of dichroic samples from a single measurement by circular polarization orthogonality breaking", Opt. Lett. **40**(7), 1270–1273 (2015).
26. F. Parnet, J. Staes, J. Fade, N. Ortega-Quijano, and M. Alouini, "Orthogonality-breaking polarimetric sensing modalities for selective polarization imaging," Opt. Lett. **45**(6), 1423–1426 (2020).
27. D. Zink, A. H. Fischer, and J. A. Nickerson, "Nuclear structure in cancer cells," Nat. Rev. Cancer **4**(9), 677–687 (2004).
28. N. Ortega-Quijano, J. Fade, M. Roche, F. Parnet, and M. Alouini, "Orthogonality-breaking sensing model based on the instantaneous Stokes vector and the Mueller calculus," J. Opt. Soc. Am. A **33**(4), 434–446 (2016).
29. F. Parnet, J. Fade, N. Ortega-Quijano, G. Loas, L. Frein, and M. Alouini, "Free-space active polarimetric imager operating at 1, 55 μm by orthogonality breaking sensing," Opt. Lett. **42**(4), 723 (2017).
30. J. Staes, F. Parnet, J. Fade, N. Ortega-Quijano, and M. Alouini, "Near-infrared active and selective polarization imaging by orthogonality-breaking: calibration of the acquisition chain (conference presentation)," in *Unconventional Optical Imaging II*, vol. 11351 (International Society for Optics and Photonics, 2020), p. 113511E.
31. N. Kireeva, M. Lakonishok, I. Kireev, T. Hirano, and A. S. Belmont, "Visualization of early chromosome condensation : a hierarchical folding, axial glue model of chromosome structure," J. Cell Biol. **166**(6), 775–785 (2004).
32. K. J. Meaburn, "Spatial genome organization and its emerging role as a potential diagnosis tool," Front. Genet. **7**, 134 (2016).
33. A. Radhakrishnan, K. Damodaran, A. C. Soylemezoglu, C. Uhler, and G. Shivashankar, "Machine learning for nuclear mechano-morphometric biomarkers in cancer diagnosis," Sci. Rep. **7**(1), 17946 (2017).
34. M. Koester, A. Mohammadi-Sangcheshmeh, M. Montag, F. Rings, T. Schimming, D. Tesfaye, K. Schellander, and M. Hoelker, "Evaluation of bovine zona pellucida characteristics in polarized light as a prognostic marker for embryonic developmental potential," Reproduction **141**(6), 779–787 (2011).
35. M. Koike-Tani, T. Tani, S. B. Mehta, A. Verma, and R. Oldenbourg, "Polarized light microscopy in reproductive and developmental biology," Mol. Reprod. Dev. **82**(7-8), 548–562 (2015).